Ab initio study of domain structures in half-metallic CoTi$_{1-x}$Mn$_x$Sb and thermoelectric CoTi$_{1-x}$Sc$_x$Sb half-Heusler alloys

Joaquin Miranda Mena[*], Heiko G. Schoberth, Thomas Gruhn, Heike Emmerich

Lehrstuhl für Material- und Prozesssimulation, Universität Bayreuth, Universitätsstraße 30, D-95447 Bayreuth, Germany

ABSTRACT

We present first-principles calculations of the electronic density of state, the structures in CoTi$_{1-x}$Sc$_x$Sb and CoTi$_{1-x}$Mn$_x$Sb. In addition for the latter we calculate magnetic moments. Systems with different stoichiometries are compared and low energy configurations are determined using a cluster expansion procedure. For all studied manganese concentrations, $x > 0$, CoTi$_{1-x}$Mn$_x$Sb is half-metallic and magnetic, which make it interesting for spintronic applications. In contrast, with increasing scandium concentration, the band gap of CoTi$_x$Sc$_{1-x}$Sb closes continuously, while the material changes from a semiconductor to a non-magnetic metal. For low Sc doping this material is well suited for thermoelectric applications. The electronic states close to the Fermi energy are strongly influenced by the distribution of Ti and Mn (or Ti and Sc). This has important consequences for the usage of materials in application fields like spintronics and thermoelectrics. In general, a phase separation of the alloys into a Ti rich and a Ti poor phase is energetically favored. Using mean field theory we create a phase diagram that shows the coexistence and the spinodal region. A spontaneous demixing can be used for the creation of nano-domains within the material. In the case of CoTi$_{1-x}$Sc$_x$Sb, the resulting reduced lattice thermal conductivity is beneficial for thermoelectric applications, while in CoTi$_{1-x}$Mn$_x$Sb the nanodomains are detrimental for polarization.

© 2015 Elsevier B.V. All rights reserved.

1. Introduction

Ever since their discovery 120 years ago [1,2], Heusler alloys have continuously offered interesting properties. The first distinctive feature was the ability to obtain magnetization from the composition of non-magnetic elements. Structurally, Heuslers (X_2YZ) are formed by four interpenetrating X, X′, Y, and Z fcc sublattices, where X and Y are transition metal elements − Y could be a rare-earth metal though − and Z is a main group element. If one sublattice is left empty, it gives rise to the half-Heusler or also called semi-Heusler (XYZ) with the C_{1b} symmetry. Electronically, there are clear connections between their diverse functionality and the complexity of their chemical bonding [3]. Moreover, half-Heuslers show a wide variety of properties. They can be semiconductors, metals, semi-metals, ferromagnets, antiferromagnets, and more [3–5]. Hence, not surprisingly, they have generated large interest not only from a fundamental point of view, but also for applications. Currently, half-Heusler materials are developed and investigated with regard to many applications, ranging from semiconductors (tunable band gaps for solar cells [7,6]) and magnetic properties (non-volatility storage of data [8]) to the emergent physics of topological insulators [9]. Two important areas are thermoelectrics and spintronics. The former focuses on the ability to harvest energy from wasted heat in thermal processes [10]. If such ability could be maximized above room temperature [11], the direct consequences in the reduction of the energy cost as well as reduction of pollution would be tremendous. The second area is driven by the ever-demanding sector of electronics. Conventionally only the electro-charge properties have been exploited, but the possibility of using the spin properties of the electrons opens novel alternatives to manufacture a new generation of electronic devices at the nano-scale level [12].

In the case of thermoelectrics, CoTiSb has attracted a lot of interest [13]. The efficiency of a thermoelectric material is characterized by the figure of merit

$$ZT = \frac{S^2\sigma}{\kappa_e + \kappa_l}T, \tag{1}$$

where S is the Seebeck coefficient, σ is the electrical conductivity and κ_e and κ_l are the electronic and the lattice thermal conductivities, respectively. While the Wiedemann–Franz law predicts that σ and κ_e are proportional, the figure of merit can be increased by decreasing the lattice thermal conductivity. It has been proposed that one way to obtain higher values of ZT is by inducing phase separation that lead to nanodomains of different composition. The domain boundaries reduce the local heat transport and scatter the phonons, leading to a reduction of κ_l. In this regard, preparation of solid solutions based on half-Heusler materials, $CoTi_{1-x}Mn_xSb$, have shown favorable results [14,15]. In particular, it was found experimentally that $CoTi_{1-x}Sc_xSb$ has a lower lattice thermal conductivity and a higher ZT than pure CoTiSb, if $0 < x \leq 0.05$ [16].

In this paper we show that the alloys Co(Ti,Sc)Sb and Co(Ti,Mn)Sb are energetically less stable than the composition of their respective parental structures CoTiSb, CoScSb, and CoMnSb. This predicts the existence of a spinodal region below a critical temperature. In this region, the material demixes spontaneously, forming nanodomains like those found experimentally for Co(Ti,Mn)Sb. Since the separated phases are more stable, a remixing of the phases and a corresponding reduction of the figure of merit is unlikely.

The half-metallicity term was coined by de Groot in his seminal paper [17] where *ab initio* calculations were performed on the half-Heusler NiMnSb. A series of publications focused on to the manifestation of half-metallicity in related alloys [18,5]. The changes in these properties were studied as vacancies or different types of disorder are introduced in quaternary compounds: $XY_{1-x}M_xZ$, where M is also a transition metal atom [22,13,19–21,23,24]. Half-metallicity is the key feature to be exploited by spintronics. This electronic state is manifested when electrons at the Fermi level (E_F) are restricted to the majority spin channel, spin-up, while at the same time the minority spin channel, spin-down, has a gap at E_F. Interestingly enough, depending on the spin channel, the Seebeck coefficient in half-metals can vary hugely [25,26]. This offers the opportunity to study from a different perspective the half-metallic ferromagnets within the context of thermoelectrics. We follow the variations of the semi-metallic state and the changes in the magnetic moments for the full range of manganese concentration in $CoTi_{1-x}Mn_xSb$, a combination of a semiconductor CoTiSb and CoMnSb, which is an archetypical half-metallic ferromagnet. We also show how the electronic properties differ locally in the demixing phase.

In this article, we investigate the alloys Co(Ti,Sc)Sb and Co(Ti,Mn)Sb with the help of first principle calculations, a cluster expansion of the energy and mean field calculations. Various concentrations, configurational, electronic, and magnetic properties are studied. The densities of states are used to predict electronic properties and help to understand the stability of the configurations. We find that configurations with separated Ti and Sc (Mn) atoms have the lowest energy. This separation on a scale of a few Angstrom indicates phase separation on larger scales. The mean field model we offer will help to clarify that indeed it exists a phase separation below 1000 K and 1400 K for Co(Ti,Sc)Sb and Co(Ti,Mn) Sb respectively. This supports, for instance, recent reports of phase-separation in Co(Ti,Sc)Sb half-Heuslers with enhanced ZT [27], while in Co(Ti,Mn)Sb, it could be related to an increase in the resistivity in close half-Heuslers systems [28].

2. Methodology

A Heusler material consists of four interpenetrating fcc sublattices A, B, C, D. In a cubic unit cell, the sublattices include the points (0,0,0), (0.25,0.25,0.25), (0.5,0.5,0.5), and (0.75,0.75,0.75), respectively, (see Fig. 1 where two adjacent unit cells are
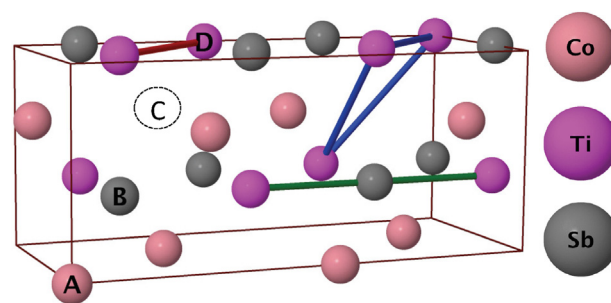

Fig. 1. Two adjacent CoTiSb unit cells with the ABD structure (A = Co, B = Ti, D = Sb, C site is empty). The relevant tuples for the ECI's interaction are depicted: The red stick connects the nearest neighbor pair, the green stick the second nearest neighbor pair and blue sticks the triplet.(For interpretation of the references to color in this figure legend, the reader is referred to the web version of this article.)

illustrated). In the half-Heusler, only three of the four sublattices are occupied. There are, in general, three distinguishable ways to distribute the components X, Y, and Z of a half-Heusler XYZ on the sublattices.

Fig. 2 shows the energies of the density functional theory (DFT) calculation for the ACD, DCB and ABD configurations of the pure materials CoTiSb, CoMnSb and CoScSb. Here, the XYZ (X, Y, $Z = A$, B, C, D) follow the same order of CoLSb ($L = Ti$, Sc, Mn). One finds that for all three pure materials, ABD has the lowest ground state energy. Results from our calculations for the pure materials can be compared with literature values. Lattice parameters and magnetic moments are in reasonable agreement with experiments and other DFT publications.[1] We obtained the lattice parameters of $a = 5.88$Å for CoTiSb, $a = 6.10$Å for CoScSb and $a = 5.82$Å for CoMnSb with magnetic moments of $\mu_{Co} = -0.15\ \mu_B$, $\mu_{Mn} = 3.19\ \mu_B$ and $\mu_{Sb} = -0.09\ \mu_B$ (all the calculated magnetic moments in CoTiSb and CoScSb were zero). We should mention that an alternative structure with a $Fm\overline{3}m$ space group has been reported for CoMnSb [32]. For Ti-rich $CoTi_{1-x}Mn_xSb$, up to $x = 0.10$ Mn could be added successfully [22].

In our calculations we investigate configurations of $CoTi_{1-x}Sc_xSb$ and $CoTi_{1-x}Mn_xSb$ that preserve the ABD atom arrangements of the parental fcc structure. A is occupied by cobalt, B either by titanium or scandium in $CoTi_{1-x}Sc_xSb$, and either by titanium or manganese in $CoTi_{1-x}Mn_xSb$; D is occupied by antimony.

In the following, the cluster expansion method is explained for the case of $CoTi_{1-x}Sc_xSb$; the alloy $CoTi_{1-x}Mn_xSb$ is treated analogously. The total configurational energy of a $CoTi_{1-x}Sc_xSb$ lattice with lattice sites i occupied by either Ti or Sc can be expressed in a cluster expansion:

$$E(\sigma) = \sum_\alpha m_\alpha J_\alpha \left\langle \prod_{i \in \alpha'} \sigma_i \right\rangle. \tag{2}$$

The pseudospin representation $\sigma_i = +1, -1$ depends on the titanium or scandium occupation. Clusters are defined by the α label, e.g. it groups a number of lattice sites i characterized by their spatial arrangement. The strength of the effective cluster interaction (ECI) is J_α, and m_α counts the multiplicity of equivalent α' clusters related to α by a symmetry operation. Hence, the set of σ_i and J_α, m_α coefficients define the energy for a given lattice configuration.

In order to calculate $E(\sigma)$, the sum must be approximated by a finite set of clusters. We choose the MIT Ab-initio Phase Stability

---

[1] $a = 5.882$Å for CoTiSb [13] and $a = 5.878$Å for CoMnSb [29]. Magnetic moments in CoMnSb using DFT $\mu_{Co} = -0.132\mu_B$, $\mu_{Mn} = 3.17\ \mu_B$ and $\mu_{Sb} = -0.098\ \mu_B$ [30].
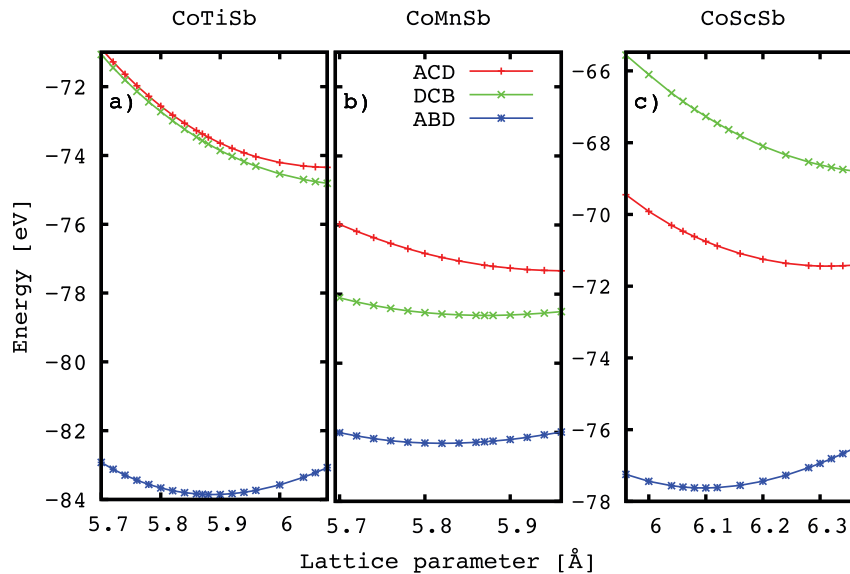
Fig. 2. The ACD, DCB and ABD configuration energy for the fcc phase on a) CoTiSb b) CoMnSb and c) CoScSb. In all cases, the lowest energy configuration is the ABD arrangement. The energies were calculated with DFT.

(maps) code, provided with the ATAT toolkit [33], to find a suitable set of clusters α and coefficients J_α. In this procedure an optimized expression for E is created with the help of energies E_i that are obtained from DFT calculations of selected configurations j. DFT calculations are performed in selected structures out of a pool of configurations suggested by the maps algorithm. If $\widehat{E}_i$ is the predicted energy for a structure i obtained from a fitting to the $(n-1)$ other structures, the so called cross-validation (CV) score is used as criterion to stop the creation of new structures and further DFT calculations:

$$CV = \left(n^{-1} \sum_{i=1}^{n} \left(E_i - \widehat{E}_i \right)^2 \right)^{1/2}. \tag{3}$$

For a formal definition of CV we refer to Stone [34] and for its implementation in the cluster expansion to van de Walle and G. Ceder [33]. A CV near 0.01 eV is considered as an acceptable score and usually it is achieved with around 30 to 50 structures [35]. We treat the alloy as a pseudo-binary system, keeping cobalt and antimony sites fixed within the cells, while titanium and scandium can swap positions for a given concentration.

The cluster expansion is of great help for finding configurations with low energy [36]. *Ab initio* studies can be strongly restricted to a small set of configurations, for which low energies are predicted.

Regarding the DFT code, we used the projector augmented wave method (PAW) [37] implemented by the Vienna ab-initio simulation package VASP. For details on the PAW potentials we refer to G. Kresse [38]. Atoms were modeled with pseudopotentials together with semi-core electrons. The electronic wave function was expanded in plane waves up to an energy cut-off of 350 eV. The Perdew–Burke–Ernzerhof generalized gradient approximation (GGA) was used as exchange potential. A 8 × 8 × 8 Monkhorst–Pack [39] k-point mesh for Brillouin integration was selected. Magnetic interactions were taken into account through spin-polarized electronic density of states − the local spin-density approximation (LSDA) − with default initial magnetic moments. For structural optimization we took into account relaxation of unit cell shape, ion positions and lattice parameters (volume of the unit cell). Force values larger than 0.005 eV/Å were allowed to relax with a maximum number of fifteen ionic steps. As for the DFT energy

convergence criteria, we set the energy difference between two successive self-consistent calculations to 0.0001 eV. The largest unit cells considered were made up of 48 atoms.

3. Structural stability

First we study the distribution of Ti and Sc (Mn). In this section we show that even though we are dealing with supercells consisting of a few unit cells, configurations with a strong separation of Ti and Sc(Mn) atoms are energetically favored.

For CoTi$_{1-x}$Sc$_x$Sb we computed with DFT 62 configurations, achieving a CV of 0.0033 eV, and for CoTi$_{1-x}$Mn$_x$Sb we computed 85 configurations with a CV of 0.0011 eV. In Fig. 3 the ECI's obtained by the fitting procedure are shown. For CoTi$_{1-x}$Mn$_x$Sb the following major contributions to the energy are found: There is a strong pair interaction for nearest neighbors and a less strong for next nearest
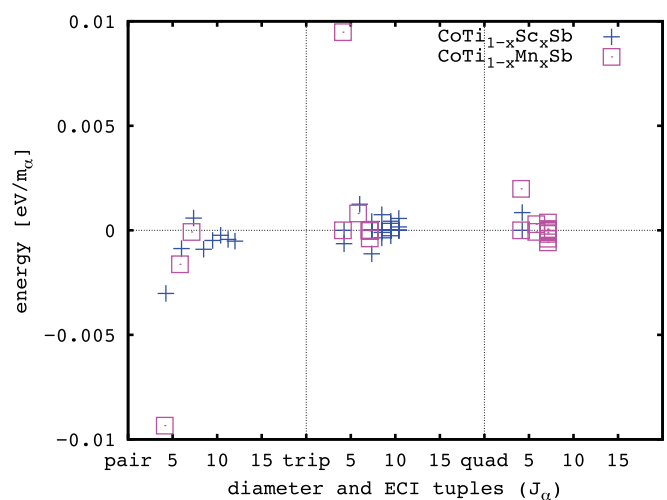

Fig. 3. The strength of ECI's for CoTi$_{1-x}$Sc$_x$Sb and CoTi$_{1-x}$Mn$_x$Sb. The first, second and third part of the graph correspond to pairs, triplets and quadruples respectively. The calculated diameter for each tuple is the maximum distance between any two sites within the cluster, it is given in Å.
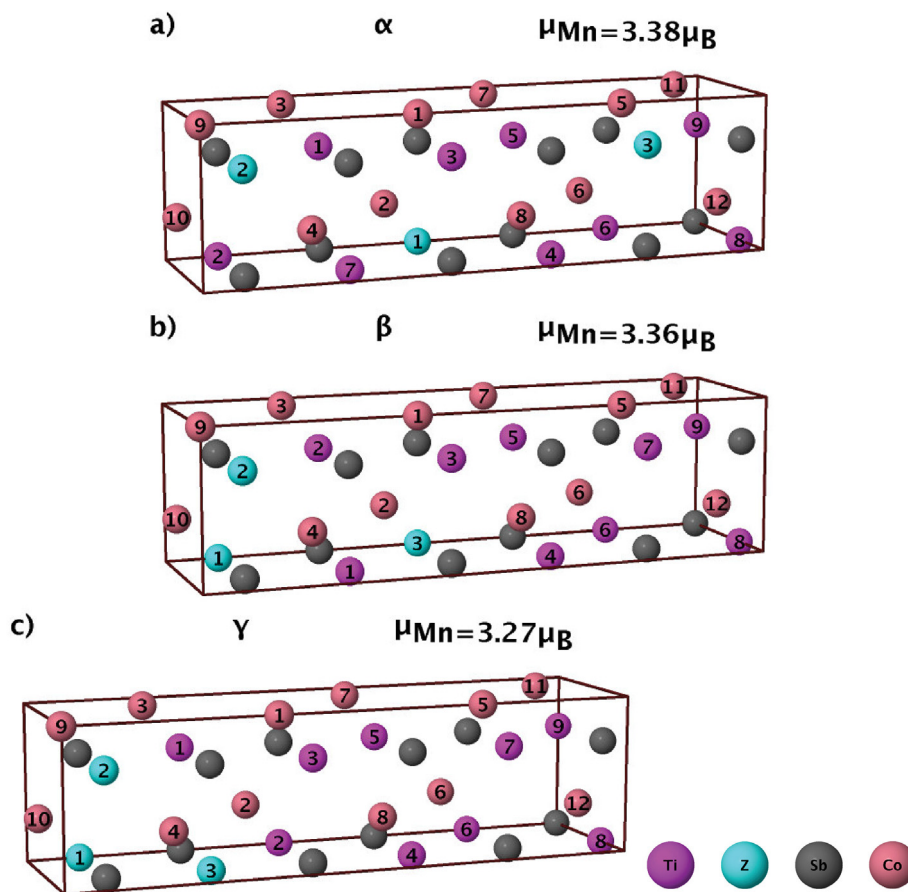
Fig. 4. Three unit cells for $CoTi_{0.75}Z_{0.25}Sb$ ($Z = Sc,Mn$) with different arrangements of titanium and Z atoms. Each unit cell consists of 36 atoms. In both cases ($Z = Mn$ and $Z = Sc$) γ is the lowest energy structure corresponding to the maximum number of manganese–manganese (scandium–scandium) nearest neighbors. Energies and magnetization calculated by DFT.

neighbor pairs. In both cases, the energy coefficient is negative, such that pairs of identical atoms are favored. The coefficient is positive for the dominant energy triplet of $CoTi_{1-x}Mn_xSb$ and it is formed by connecting three contiguous atoms, which together shape an equilateral triangle with a nearest neighbor distance as a side-length. The former relevant tuples are illustrated in Fig. 1. A quadruplet is also found for both systems, but with a weaker contribution. ECIs for $CoTi_{1-x}Sc_xSb$ are distinctly weaker, but a larger number of pair and triple clusters is considered.

3.1. $CoTi_{1-x}Sc_xSb$

We start with a comparison of three structures α, β, and γ of $CoTi_{0.75}Sc_{0.25}Sb$, as shown in Fig. 4. In the α configuration, the Sc atoms have the largest distance, while in the γ configuration, Sc and Ti atoms are separated. The closer the Sc atoms are packed together, the lower is the energy of the system, $E(\alpha) > E(\gamma) > E(\beta)$. This indicates that a separation of Sc and Ti atoms is favored (see Table 1).

In Fig. 5 different configurations of $CoTi_{0.5}Sc_{0.5}Sb$ are depicted. Fig. 5a shows the structure with the largest distance between the Sc atoms, while in 5c the Sc atoms are close to each other. Again, larger separations of Ti and Sc leads to lower energies, $E(\alpha') > E(\gamma') > E(\beta')$, see Table 1.

3.2. $CoTi_{1-x}Mn_xSb$

Also in the case of Mn doping, $CoTi_{0.75}Mn_{0.25}Sb$, one has $E(\alpha)$

$> E(\gamma) > E(\beta)$ (see Fig. 5 and Table 1), as well as in $CoTi_{0.75}Mn_{0.25}Sb$ (see Fig. 4 and Table 2). The structures are magnetic and compact Mn regions present the lowest magnetization. The total magnetization of the α, β and γ structures calculated by DFT are 8.77 μ_B, 8.78 μ_B and 8.82 μ_B respectively. The manganese atoms have an average magnetic moment of 3.38 μ_B, 3.36 μ_B, and 3.27 μ_B respectively for α, β and γ. Note that larger distances between manganese atoms increase the magnetic moments.

The same behavior is found by comparing $CoTi_{1-x}Mn_xSb$ compounds with different manganese concentration. For low x, for which the average distance between manganese atoms is large, the

Table 1
Configurational energy of the three $CoTi_{1-x}Z_xSb$ ($x = 0.25, 0.5$; $Z = Sc, Mn$) structures shown in Figs. 4 and 5. Magnetic moments for $Z = Mn$ are also listed. Energy values denote the difference to the γ (γ') structure.

Structure	$CoTi_{0.75}Sc_{0.25}Sb$ energy (eV)	$CoTi_{0.75}Mn_{0.25}Sb$	
		Energy (eV)	$\mu(\mu_B)$
α	0.155	0.829	3.38
β	0.052	0.330	3.33
γ	0.00	0.0	3.27
Structure	$CoTi_{0.50}Sc_{0.50}Sb$ Energy (eV)	$CoTi_{0.50}Mn_{0.50}Sb$	
		Energy (eV)	$\mu(\mu_B)$
α'	0.113	0.311	3.34
β'	0.041	0.186	3.33
γ'	0.00	0.0	3.28

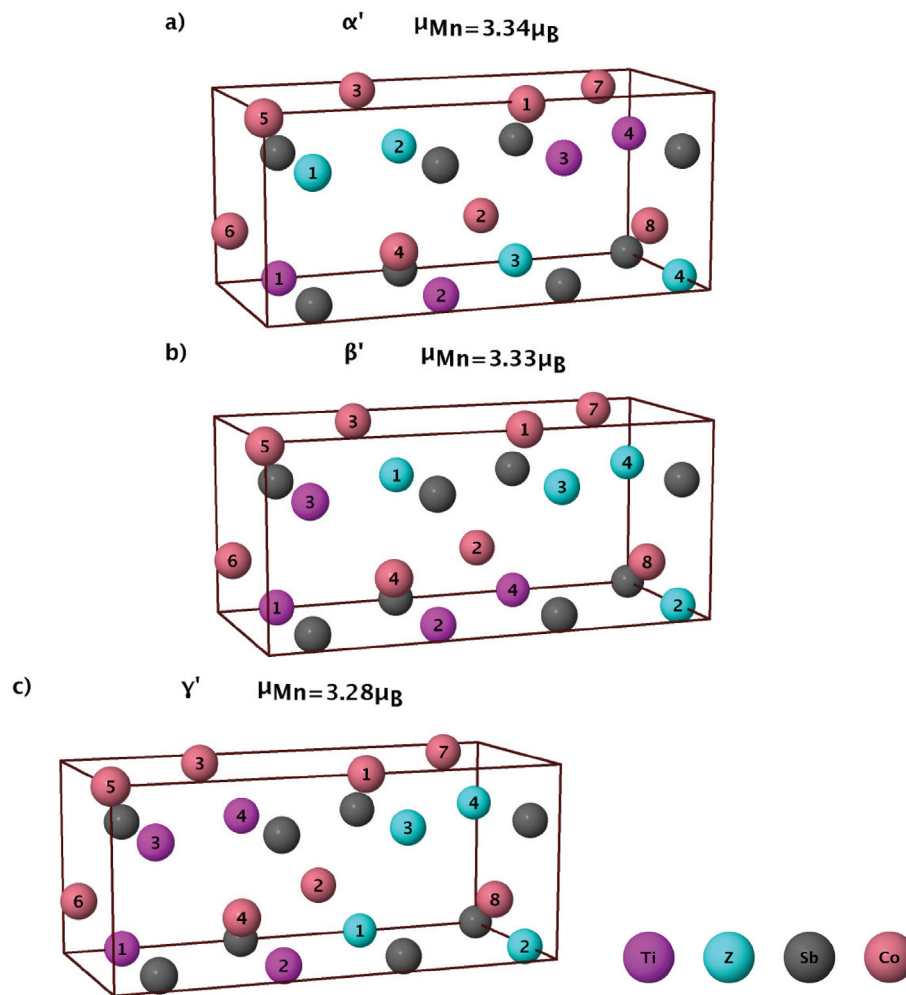**Fig. 5.** Three unit cells for $CoTi_{0.5}Z_{0.50}Sb$ ($Z = Sc,Mn$) with different arrangements of titanium and Z atoms. Each unit cell consists of 24 atoms. In both cases ($Z = Mn$ and $Z = Sc$), γ' is the lowest energy structure corresponding to the total separation of titanium from manganese (scandium). This gives rise to a sub-unit cell of pure CoTiSb, see the half right of the unit cell, and one pure CoMnSb (CoScSb) sub-unit cell, see the half left of the unit cell. α' and β' with a more homogeneous atomic distribution have higher energies. Energies and magnetization calculated by DFT.

magnetic moment of the Mn atoms is high. As an example, magnetic moments are shown in Table 2 ($x = 0.125$) and Table 3 ($x = 0.875$) together with the atomic position of all atoms in the unit cells of $CoTi_{1−x}Mn_xSb$. The single manganese atom in $CoTi_{0.875}Mn_{0.125}Sb$ has a magnetic moment of 3.38 μ_B, the seven manganese atoms in $CoTi_{0.125}$ $Mn_{0.875}$ Sb have moments of 3.21 μ_B or 3.22 μ_B. In addition, titanium changes its average magnetic moment of -0.02 μ_B at a Mn concentration $x = 0.125$ to -0.29 μ_B at $x = 0.875$. Finally, some Cobalt atoms have stronger magnetic moments (between $\mu = -0.17$ μ_B and -0.21 μ_B) in the case of $x = 0.875$. Manganese couples anti-ferromagnetically to the other type of the atoms. Putting together this information, we can infer that moment values of Mn are transferred to Co and Ti, as more Mn is introduced, but with opposite spin polarization. The reason for this behavior is most likely found in the strong hybridization between Co and Mn, combined with an indirect exchange mechanism among Mn atoms which is mediated by Sb [40].

3.3. DFT structural energy diagram

Fig. 6 shows the configurational energy divided by the number of atom sites. Red crosses denote DFT calculations, while green squares are results of the cluster expansion. In almost all cases, the

two values are in good agreement, corresponding to the low CV. One finds that for all concentrations x the alloys are less stable than the corresponding pure states. Thus, the mixed system has a phase coexistence region, in which the system favors a demixing of Ti and Mn (or Ti and Sc) in their sublattice. This demixing occurs as the alloy is cooled down below the critical temperature. For the case of Co(Ti,Mn)Sb [14] this demixing has been found experimentally. As the system is cooled down further, the demixing dynamics finally freeze in, as the exchange rates of ions between the sites gets low. The domains formed by the decomposition process are of great advantage for thermoelectric applications as they reduce the lattice thermal conductivity [41]. The degree of demixing depends on the cooling process, since diffusion of atoms is strongly reduced at low temperatures. The degree of mixing in the sublattice influences the heat conductivity but also the electronic properties. In the following we study the electronic structure, depending on the stoichiometry and the atom configuration.

4. Density of states

The Seebeck coefficient and the electrical conductivity (σ) are properties that depend strongly on the electronic structure. The density of states (DOS) in the vicinity of the Fermi level has a strong

Table 2
Atom positions and individual magnetic moments within the unit cell of $CoTi_{0.875}Z_{0.125}Sb$ (Z = Sc, Mn). Lattice vectors are defined by: $[\vec{a}; \vec{b}; \vec{c}] = [0, -L, 0; 0, 0, -L; 2L, 0, 0]$ with L = 5.911 for Z = Sc and L = 5.885 for Z = Mn.

Atom	$CoTi_{0.875}Sc_{0.125}Sb$			$CoTi_{0.875}Mn_{0.125}Sb$			$\mu(\mu_B)$
	x	y	z	x	y	z	
Co_1	0.000	0.000	0.501	0.000	0.000	0.500	0.0
Co_2	0.500	0.500	0.501	0.500	0.500	0.500	0.0
Co_3	0.006	0.494	0.254	0.000	0.500	0.250	−0.07
Co_4	0.494	0.006	0.254	0.500	0.000	0.250	−0.06
Co_5	0.006	0.006	−0.004	0.000	0.000	0.000	−0.06
Co_6	0.494	0.494	−0.004	0.500	0.500	0.000	−0.05
Co_7	0.000	0.500	0.749	0.000	0.500	0.750	0.0
Co_8	0.500	0.000	0.749	0.500	0.000	0.750	0.0
Sb_1	0.250	0.250	0.378	0.250	0.250	0.375	−0.01
Sb_2	0.750	0.750	0.377	0.750	0.750	0.375	−0.01
Sb_3	0.250	0.750	0.125	0.250	0.750	0.125	−0.01
Sb_4	0.750	0.250	0.125	0.750	0.250	0.125	−0.01
Sb_5	0.250	0.250	0.872	0.250	0.250	0.875	−0.01
Sb_6	0.750	0.750	0.873	0.750	0.750	0.875	0.0
Sb_7	0.250	0.750	0.625	0.250	0.750	0.625	0.0
Sb_8	0.750	0.250	0.625	0.750	0.250	0.625	0.0
Ti_1	0.250	0.250	0.125	0.250	0.250	0.125	−0.06
Ti_2	0.750	0.250	0.375	0.750	0.250	0.375	−0.04
Ti_3	0.250	0.750	0.375	0.250	0.750	0.375	−0.03
Ti_4	0.750	0.750	0.625	0.750	0.750	0.625	0.03
Ti_5	0.250	0.250	0.625	0.250	0.250	0.625	0.0
Ti_6	0.750	0.250	0.875	0.750	0.250	0.875	−0.04
Ti_7	0.250	0.750	0.875	0.250	0.750	0.875	−0.03
Z	0.750	0.750	0.125	0.750	0.750	0.125	3.38

Fig. 6. Energy per site for several $CoTi_{1-x}Z_xSb$ configurations with a) Z = Sc, b) Z = Mn. Red crosses denote DFT calculations, while green squares are results of the cluster expansion. The ground states are set as reference energies. The energies for the structures α, β, and γ, shown in Fig. 4 (α', β', and γ' respectively in Fig. 5), are indicated. (For interpretation of the references to color in this figure legend, the reader is referred to the web version of this article.)

impact on these quantities. The combination of both defines the power factor ($S^2\sigma$), which is proportional to ZT (see Eq. (1)). Typically, thermoelectric materials are semiconductors which are doped to be n- or p-type. Thus, previous works have investigated the effects of modifying the DOS with doping and its consequences on S and σ [27,20,43]. For spintronic applications a metallic state in one spin channel and a semiconducting in second channel is required. It is desirable that the latter channel has a complete

Table 3
Atom positions and individual magnetic moments within the unit cell of $CoTi_{0.125}Z_{0.875}Sb$ (Z = Sc, Mn). Lattice vectors are defined by: $[\vec{a}; \vec{b}; \vec{c}] = [L, 0, -L; L, -L, 0; 0, -L, -L]$ with L = 6.064 for Z = Sc and L = 5.830 for Z = Mn.

Atom	$CoTi_{0.125}Sc_{0.875}Sb$			$CoTi_{0.125}Mn_{0.875}Sb$			$\mu(\mu_B)$
	x	y	z	x	y	z	
Co_1	−0.015	0.005	0.005	−0.004	0.001	0.001	−0.17
Co_2	0.000	0.000	0.500	0.000	0.001	0.500	−0.04
Co_3	0.000	0.500	0.500	0.000	0.500	0.500	−0.03
Co_4	0.505	0.005	0.485	0.501	0.001	0.496	−0.21
Co_5	0.500	0.500	0.500	0.501	0.500	0.500	−0.04
Co_6	0.505	0.485	0.005	0.501	0.496	0.001	−0.19
Co_7	0.505	0.005	0.005	0.501	0.001	0.001	−0.19
Co_8	0.000	0.500	−0.000	−0.000	0.500	0.001	−0.03
Sb_1	0.873	0.877	0.377	0.877	0.873	0.377	−0.07
Sb_2	0.873	0.877	0.877	0.877	0.873	0.873	−0.07
Sb_3	0.873	0.373	0.877	0.877	0.377	0.873	−0.07
Sb_4	0.375	0.875	0.875	0.375	0.875	0.875	−0.08
Sb_5	0.377	0.373	0.877	0.373	0.377	0.873	−0.07
Sb_6	0.377	0.373	0.373	0.373	0.377	0.377	−0.07
Sb_7	0.377	0.877	0.373	0.373	0.873	0.377	−0.07
Sb_8	0.625	0.125	0.125	0.875	0.375	0.375	−0.08
Ti_1	0.875	0.375	0.375	0.625	0.125	0.125	−0.29
Z_1	0.624	0.626	0.124	0.625	0.625	0.125	3.38
Z_2	0.624	0.626	0.626	0.625	0.625	0.625	3.21
Z_3	0.624	0.124	0.626	0.625	0.125	0.625	3.21
Z_4	0.125	0.625	0.625	0.125	0.625	0.625	3.21
Z_5	0.126	0.124	0.626	0.125	0.125	0.625	3.22
Z_6	0.126	0.124	0.124	0.125	0.125	0.125	3.21
Z_7	0.126	0.626	0.124	0.125	0.625	0.125	3.22

absence of electronic states, while the former is maximized. In this section, we characterize the electronic structure of the demixing state and compare it with its homogeneous counterpart.

We consider configurations of lowest energy for $CoTi_{1-x}Z_xSb$ with Z = Mn, Sc and x = 0.125, 0.50, 0.875. The list with the corresponding atomic coordinates within the unit cells is shown for x = 0.125 in Table 2 and for x = 0.875 in Table 3. Note the slight displacements of some atoms with respect to the perfect A, B, D positions. For x = 0.5 the atom positions are displayed in Fig. 5c. Fig. 7 shows their spin-projected DOS together with the cases of concentration x = 0 and x = 1 (pure states CoTiSb, CoScSb and CoMnSb).

4.1. $CoTi_{1-x}$ Mn_xSb

At x = 0 an equal number of spin up and down exist and they overlap in the same range of energy. Following the shape of DOS in $CoTi_{1-x}$ Mn_xSb, one observes that as more manganese is placed, there is an increase of the spin up states between $E - E_F$ = 2.7 eV and 1 eV. At x = 0.125, the DOS shows a peak at the Fermi level for spin up electrons so that the system becomes half-metallic. The half-metallicity is found for all finite Mn concentrations. The increase of the peak at −2.7 eV is due to the d-states of the Mn atoms; the role of Mn in the magnetization and half-metallicity is found in Ref. [42], while a discussion about the origin of the gap for the spin minority is given in Ref. [30].

Next we describe the effect homogeneity of the transition metal (TM) atoms onto the DOS. We have plotted in Fig. 8 the DOS of $CoTi_{0.75}$ $Mn_{0.25}$ Sb for the α and γ structures (refer to Figs. 4 and 6); it is seen that their DOS are similar across the whole range of energy. However, for $CoTi_{0.75}$ $Mn_{0.25}$ Sb, at the Fermi level: the α structure has a sharper peak than γ (Fig. 8a). The latter structure has a more spread DOS near the E_F with around 50% less available states at $E = E_F$. In addition, α presents a gap above the E_F, between 0.25 eV and 0.70 eV, while for γ the gap is closed. Since α and γ differ only in the position of manganese and titanium, it indicates that their distribution is pivotal for the inter-atomic states and the
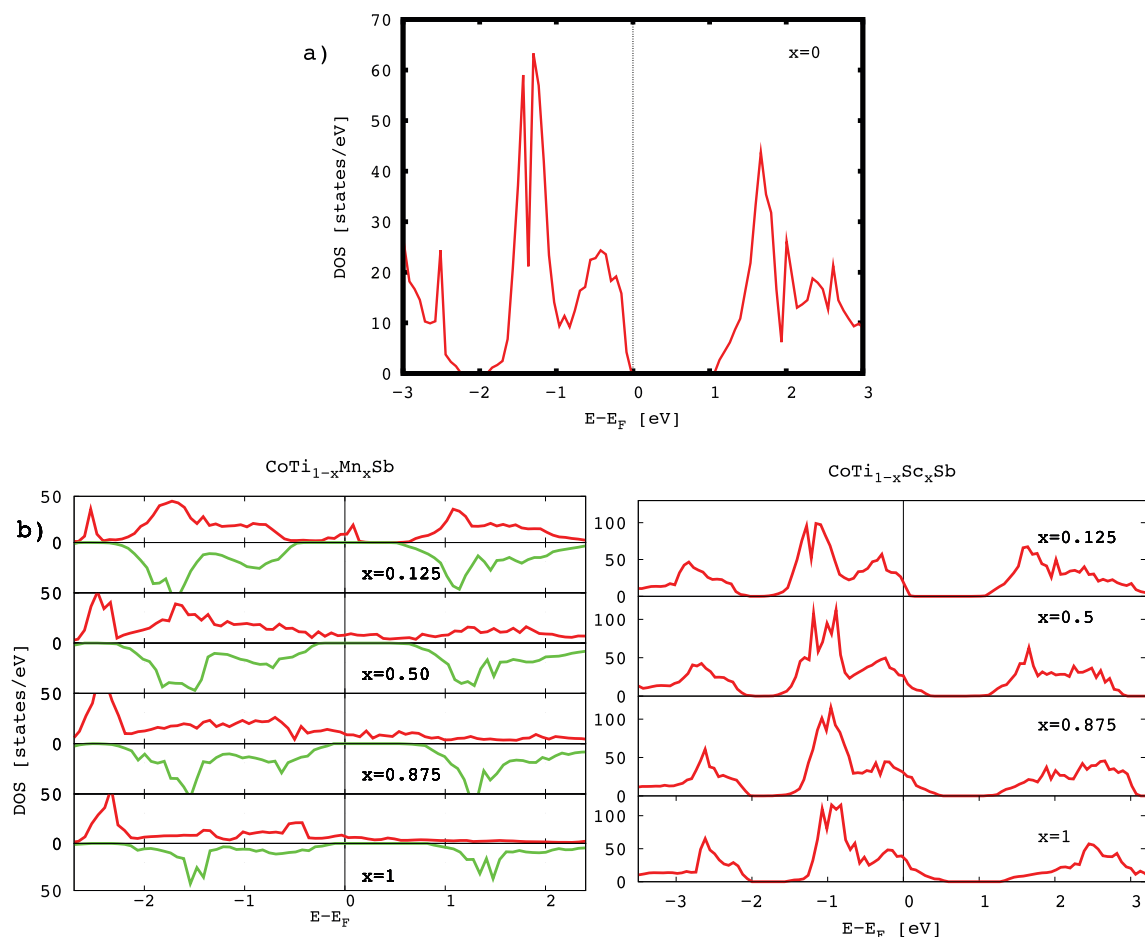
Fig. 7. a) Total DOS of CoTiSc. b) Total DOS as the concentration (x) of scandium is increased in CoTi$_{1-x}$Mn$_x$Sb (left column) and of manganese in CoTi$_{1-x}$Sc$_x$Sb (right column). The corresponding unit cells and magnetic moments are shown in Tables 2 and 3 for $x = 0.125$, 0.875. In Fig. 5c, the unit cell for $x = 0.5$ is shown.
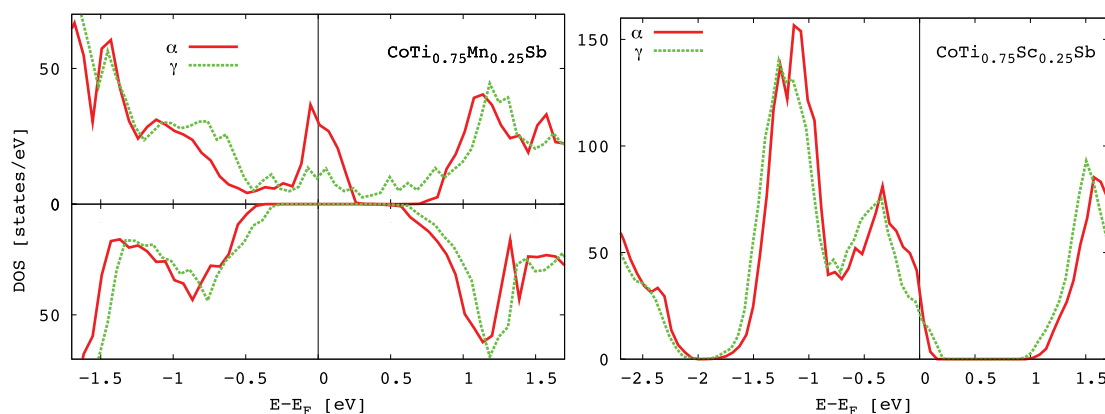

Fig. 8. Spin-projected DOS for two selected structures, high (α) and lowest energy (γ) (see Fig. 4), in CoTi$_{0.75}$Mn$_{0.25}$Sb (left panel) and CoTi$_{0.75}$Sc$_{0.25}$Sb (right panel).

resulting DOS; if manganese atoms are spread homogeneously, the electronic states with energies around E_F are more localized. This can be analyzed with the aid of the local-projected DOS, Fig. 9. In the following atoms are denoted by their type and the number, for instance Mn$_2$ is a Mn atom with number 2. In configuration α all manganese atoms are surrounded by titanium atoms on the same sublattice, (see Fig. 4) and each titanium has two manganese atoms. The result of such an even atomic distribution is that all TM atoms

contribute similarly to the DOS (Fig. 9a and b). In contrast γ, with a three manganese cluster has a flatter DOS in the range [−0.5 eV, 1.0 eV]. In γ the contribution at E_F, see Fig. 9c, is exclusively from the TM atoms placed in the Mn-rich region, like Mn$_2$, Ti$_1$ and Co$_{10}$. The situation is different for Ti$_6$ and Co$_5$ whose positions are in the Mn-free region. For these atoms, the DOS shows a large gap around E_F (Fig. 9d). The DOS is similar to that of pure CoTiSb, although the Fermi energy lies in the middle of the band gap, rather than at the
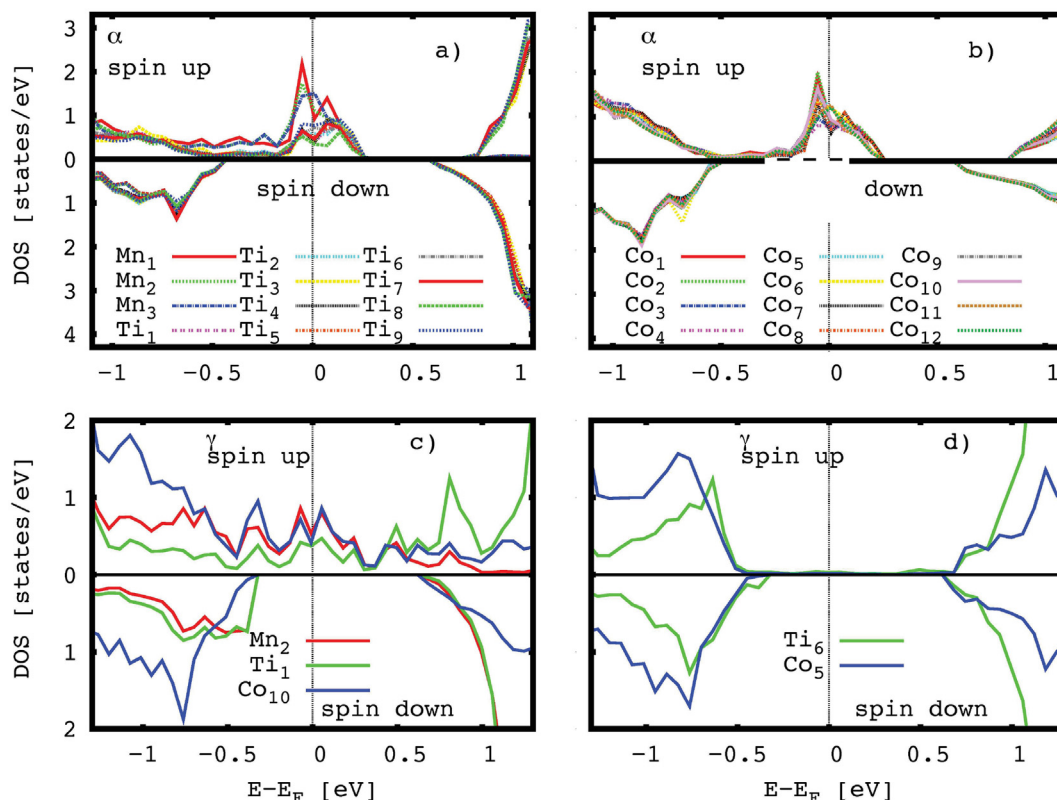
Fig. 9. *d*-local-spin projected DOS of α and γ structures in CoTi$_{0.75}$ Mn$_{0.25}$ Sb. α: a) For all three Mn and nine Ti; b) For all twelve Co. γ: c) selected Mn, Ti and Co; d) selected Ti and Co. Atom numbers refer to atom labels of Fig. 4.

lower end (compare with Fig. 7).

4.2. CoTi$_{1-x}$Sc$_x$Sb

With increasing Sc concentration, see Fig. 7, the lower end of the band gap moves to higher energies and the material changes from a semiconductor with a gap of 1.1 eV to a conductor. With respect to up and down spin states, the DOS remains symmetric for all Sc concentrations and no significant magnetism is present.

Similar to CoTi$_{0.75}$Mn$_{0.25}$Sb, we see in Fig. 8 that for the γ configuration of CoTi$_{0.75}$Sc$_{0.25}$Sb, it has also a slight reduction of states at E_F as well as a narrower gap above E_F. In the α configuration, atoms are homogeneously spread, such that all Co atom (and all Ti, Sc, Sb atoms, respectively) are surrounded by the same types of atoms. Thus, the DOS of each atom does not depend on its position; however, the DOS of different types of atoms differ strongly. The DOS of all Ti atoms and all Co atoms of the α configuration are shown in Fig. 10a and Fig. 10b, respectively. The scandium atoms show a very low DOS in the presented energy range and therefore they are not shown.

On the contrary, for the γ configuration the DOS depends strongly on the position as well as the type of each TM atom. For atoms in a more Sc-rich region, such as Sc$_2$, Ti$_1$ and Co$_{10}$, the DOS at E_F is larger (Fig. 10c) than the DOS of atoms in a Sc-poor region, such as Ti$_6$ and Co$_5$, with lower number of states at E_F (Fig. 10d).

4.3. Diluted concentrations and larger demixing volumes

Here, we study a system with diluted Z distribution, see Fig. 11, and a system of larger domains of Z-rich and Z poor phases, see Fig. 12, which is typical for heterostructures [46].

A system of CoTi$_{0.5}$Z$_{0.5}$Sb (Z = Sc, Mn) tends to demix into two phases, one with a high amount of Z and one with a diluted

concentration of Z. On the way to a macroscopically demixed state, the system forms growing domains of Z rich and Z poor composition. If the system cools down during demixing, it gets in a heterostructure.

In Fig. 12 we set a supercell composed by six sub-unit cells. Three of them are made exclusively by Sc (Mn) atoms, the other three by Ti-atoms. It is equivalent to half-doping of Sc (Mn). We focus on three regions. The first region is deep inside the Sc (Mn) volume. We select the atom with label Z_2. The second region is in the Ti volume and the atom selected is Ti$_2$. (In the first region the Z_2 atom has the maximum separation from the Ti atoms, and vice versa, in the second region Ti$_2$ has the maximum separation from the Sc (Mn) atom). The third region is in the interphase like Z_1 that lies within the edge of the Sc (Mn) volume and Ti$_1$ within the edge of the Ti-volume. The respective DOS for each region is plotted in Fig 14 for CoTi$_{1-x}$Sc$_x$Sb and in Fig 15 for CoTi$_{1-x}$Mn$_x$Sb.

4.4. CoTi$_{1-x}$Sc$_x$Sb

For the structures of Fig. 11, the total DOS corresponds to a metallic material, see Fig. 13a for CoTi$_{0.83}$ Sc$_{0.16}$ Sb. The two Sc atoms are the driving elements that leads to a metallic system as deduced from the DOS of Fig. 13b (since the two are equivalent, we only plot the DOS of Sc$_1$). This shows that if Sc atoms reduce their distance, more DOS at the Fermi level appear at and at the same time Ti atoms gain DOS at the Fermi level when they are located near the Sc atoms.

The total DOS in 14a shows that CoTi$_{0.5}$Sc$_{0.5}$Sb preserves the characteristic DOS of a conductor, but with a narrower gap above the Fermi level, if compared with the equivalent DOS of Fig. 7 corresponding to the structure at half-doping with lesser sub-unicells (Fig. 5). Regardless of the type of atom, we see in Fig. 14c and d, that electronic states appear at the Fermi level when the
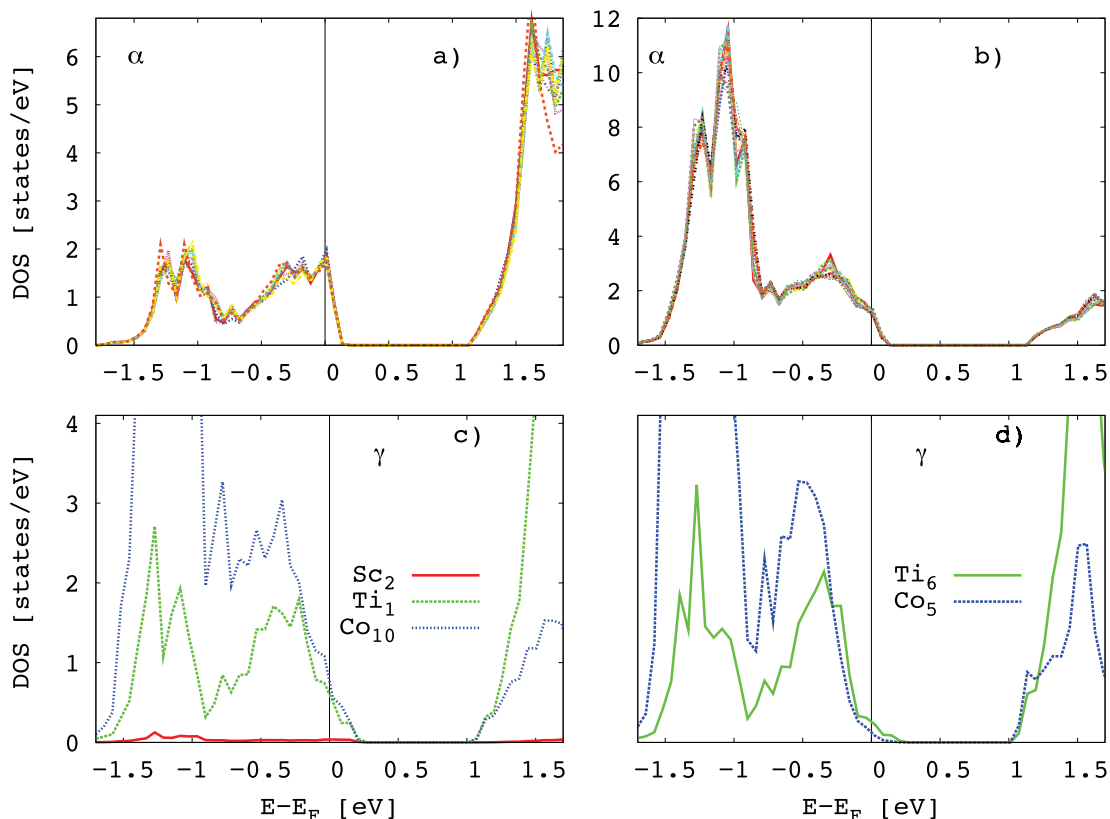
Fig. 10. d-local-spin projected DOS of α and γ structures in $CoTi_{0.75}Sc_{0.25}Sb$. α: a) For all nine Ti; b) For all twelve Co. γ: c) selected Sc, Ti and Co; d) selected Ti and Co. Atom numbers refer to atom labels of Fig. 4.
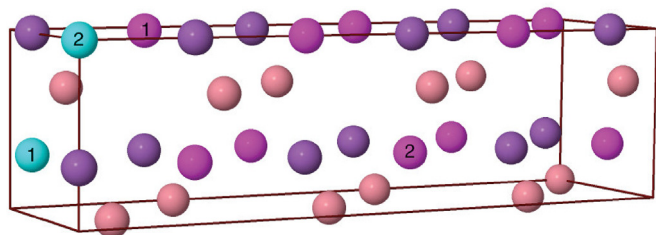

Fig. 11. Structure with diluted Z concentration (Z = Sc, Mn), $CoTi_{0.83}Z_{0.16}Sb$.

atoms are localized near the Sc–Ti interface, such as Sc_1, Ti_1, Co_1, Co_3 and Co_4. However it should be noticed that Sc atoms have a much lower contributions than Ti atoms. Atoms localized more inside the Sc-region, as Sc_2, and inside the Ti-region, as Ti_2 show a DOS of a semi-conductor with the Fermi level near the top of the valance states. The DOS of a Co atom placed deep inside the Ti region, Co_2, adopts fully the semiconducting character of the Ti atoms, while Co_5 inside the finite Mn region has a finite DOS at the Fermi level.

4.5. $CoTi_{1-x}Mn_xSb$

As in $CoTi_{0.83}Sc_{0.16}Sb$ we observe in 13c, that the small concentration of Mn atoms has a strong influence on the DOS at the Fermi level. For instance Ti_2 has almost the same DOS at E_F as the Mn atoms in $CoTi_{0.83}Mn_{0.16}Sb$, see Fig. 13d, but its DOS is much larger than that of with Sc in $CoTi_{0.83}Sc_{0.16}Sb$. In $CoTi_{0.86}Mn_{0.13}Sb$, Ti atoms far from Mn present a large gap of around 1.1 eV which includes the E_F; these Ti atoms have shifted their states towards higher energies. In general, these examples we have chosen in both systems, $CoTi_{0.83}Z_{0.16}Sb$ (Z = Mn, Sc), allow to conclude that it is not necessary to have large Sc (Mn) clusters to increase the Ti DOS around E_F in diluted samples.

The DOS in 15a shows that $CoTi_{0.5}Mn_{0.5}Sb$ remains semi-metallic, as it was the case of the half-doping with two sub-unit cells (see Figs. 5 and 7), but with an important difference in the spin-down DOS, the gap formed by states in the larger supercell present a narrower gap. The first local-spin DOS we analyze is for the Mn atoms, 15b. Here we observe that independent of the position of the manganese atoms, they always present a semi-metallic character as is seen for Mn_1 and Mn_2. The Ti-atoms present a
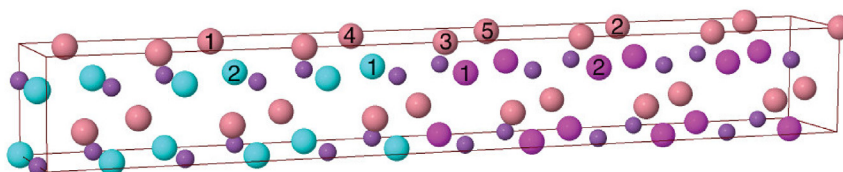

Fig. 12. Supercell (six sub-unit cells) with large volumes of exclusive Ti or Z atoms with a $CoTi_{0.5}Z_{0.5}Sb$ (Z = Sc, Mn) composition.
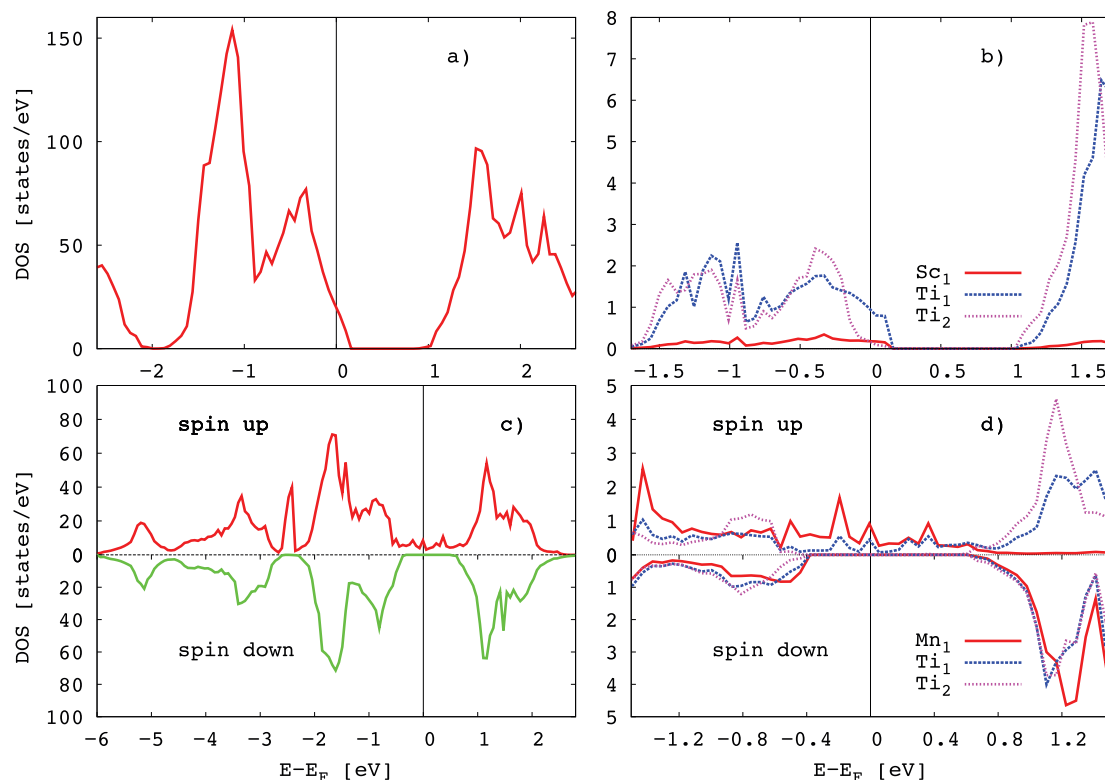
Fig. 13. a) and b) are the total DOS and site-projected DOS of Fig. 11 for CoTi$_{0.86}$Sc$_{0.13}$Sb. b) and c) are the total DOS and spin-site-projected DOS for CoTi$_{0.86}$Mn$_{0.13}$Sb.

significant variation deep inside the Ti-region. For instance deep inside the Ti-region, the Ti$_2$ has its proper semi-conducting character, while Ti$_1$ has rather a semi-metallic character. For the Co atoms, the DOS varies strongly depending on the position of the atom. Co atoms in a Mn domain, as Co$_1$ and Co$_4$ or at the domain boundary of the edge of the Mn-region, Co$_3$, have a semi-metallic DOS, the Co atoms whose environment is of Ti atoms, as Co$_2$ and Co$_5$, have a semiconductor DOS.
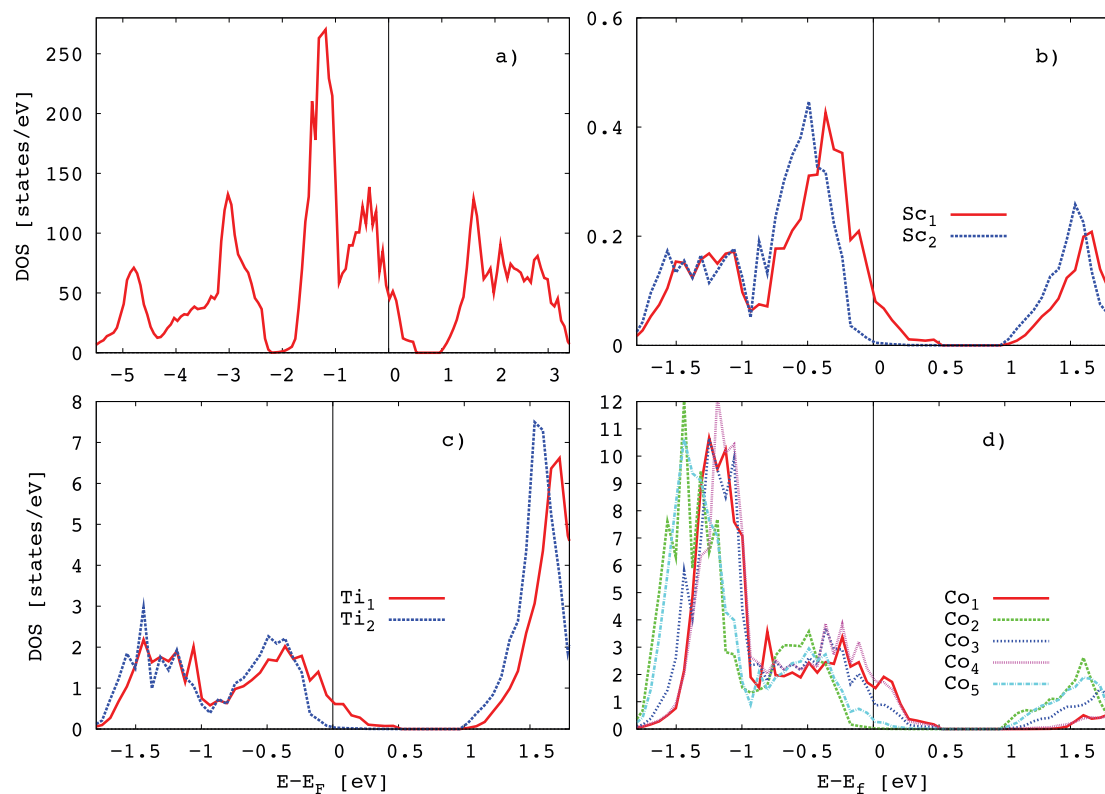

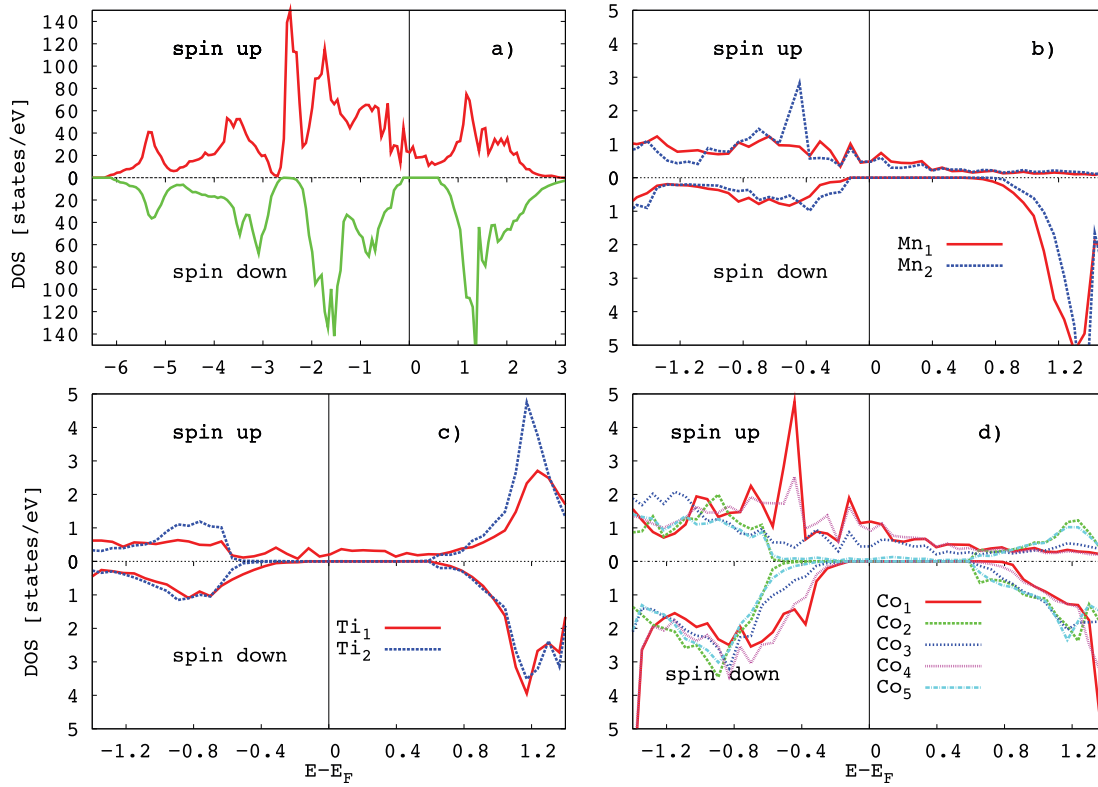**Fig. 14.** Site-projected DOS of Fig. 12 for CoT$_{0.5}$Sc$_{0.5}$Sb.

Fig. 15. Local-spin projected DOS of Fig. 12 for $CoTi_{0.5}Mn_{0.5}Sb$.

5. Mean field

In the previous section we showed that on the scale of a few Angstroms, the Sc (Mn) and Ti prefer to demix. This indicates that at larger scales the system may undergo a phase separation. In order to substantiate this, we use a mean field model to obtain a phase diagram as a function of the concentration, x, and the temperature. The aim is to localize miscibility gaps. Here we look for miscibility gaps formed in the temperature and the concentration phase diagram. The mean field model uses effective interactions taken from the coefficients of the cluster expansion explained in the Section 4.

We consider a mean field lattice model with a value s_i at each lattice site i of the (Ti,Z) sublattice is considered. The values $s_i = 1$ or -1 represent a Ti or Z occupation of site i. The state of the total lattice is determined by $\{s_c\} = (s_1, s_2, \dots s_N)$ where N is the number of lattice sites occupied by Ti or Z. The model is used to study the stability of a mixed (Ti,Z) sublattice with respect to coexisting Ti-rich and Ti-poor Co(Ti,Z)Sb states; other possible phases are neglected for simplicity.

The Hamiltonian with up to 4-body interactions is given by:

$$H = \sum_{\alpha_1=1}^{m_1} m_{\alpha_1}^{(1)} J_{\alpha_1}^{(1)} \sum_{i=1}^{N} s_i + \sum_{\alpha_2=1}^{m_2} m_{\alpha_2}^{(2)} J_{\alpha_2}^{(2)} \sum_{i=1}^{N} s_i s_j + \sum_{\alpha_3=1}^{m_3} m_{\alpha_3}^{(3)} J_{\alpha_2}^{(3)}$$
$$\times \sum_{i=1}^{N} s_i s_j s_k + \sum_{\alpha_4=1}^{m_4} m_{\alpha_4}^{(4)} J_{\alpha_2}^{(4)} \sum_{i=1}^{N} s_i s_j s_k s_r, \tag{4}$$

where m_{α_l} defines the number of clusters α_l, having an interaction strength J_{α_l} and a multiplicity $m_{\alpha_l}^{(l)}$ with $l-$ body interactions $l = 1,2,3,4$. The fixed structure of α determines the site j of s_i or sites j, k and r of s_j, s_k and s_r for a given site i of s_i. The related sites for a doublet are i,j and for a triplet i,j,k. Only one α_l is considered for a set of n-tuples, for instance for a triplet, α_3 is considered explicitly for the one set of i,j,k, the remainder is inside the multiplicity. It can be

shown, see for example [31], that the average energy is simplified as

$$\langle H \rangle_0 = N \sum_l^4 Q_l (2P - 1)^l. \tag{5}$$

with P defined as the lattice site probability of being occupied by $\sigma = 1$, and Q_l defined as

$$Q_l = \sum_{\alpha=l}^{m_l} m_\alpha^{(l)} J_\alpha^{(l)}. \tag{6}$$

We have a free energy expression in the mean field approximation:

$$F = <H>_0 - TS, \tag{7}$$

where S is the entropy given by:

$$S = -k_B N(P Log(P) + (1 - P) Log(1 - P)). \tag{8}$$

In this way we have also included configurational entropy. Note that for simplicity electronic entropy is not considered. With Eq. (7) the coexistence for Ti rich and Ti poor phases can be constructed with the double tangent method. Using the coefficients of the cluster expansion obtained in Section 3 for the $CoTi_{1-x}Sc_xSb$ and $CoTi_{1-x}Mn_xSb$ we obtain the two phase diagrams shown in Fig. 16.

The mean field results reproduced two of the main features observed in the structural energy diagram of the DFT calculations (Fig. 6): 1) The higher peak in the convex curve seen in Fig. 6b for $CoTi_{1-x}Mn_xSb$ than for $CoTi_{1-x}Sc_xSb$ in Fig. 6a is reflected in a higher critical temperature $T_c = 1400$ K for $CoTi_{1-x}Mn_xSb$ than for $CoTi_{1-x}Sc_xSb$ ($T_c = 1000$ K); 2) The coexistence lines and the spinodal are no symmetric with respect to $x = 0.5$. The maximum is approximately at $x = 0.5$. Note that, in Fig. 16, solid-fluid melting
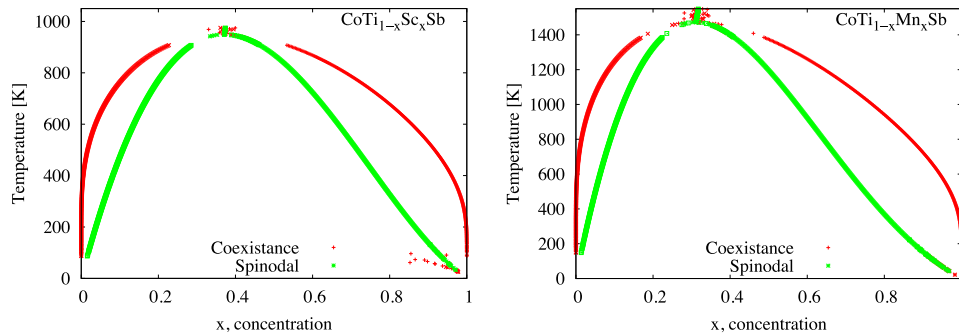
Fig. 16. Mean field phase diagram for $CoTi_{1-x}Sc_xSb$ (left) and $CoTi_{1-x}Mn_xSb$ (right). Gaps in the curves and sparce points are due to the lack analicity in the evaluated concentrations.

transitions are not considered. Most half-Heusler materials of the investigated kind have a melting temperature that is distinctly larger than 1000 K (see Ref. [47]).

In the following, the concentration which corresponds to the highest temperature T_c is denoted with x_c.

In the equilibrium state, a Ti-poor and a Ti-rich phase coexist connected by a minimum contact area. In practice, the alloys show a pattern of Ti-rich and Ti-poor domains. This is a consequence of the production process in which, for example by arc-melting, the material is created at high temperature. Then it is cooled down and enters the coexistence region in which a demixing process sets in. After a while, the material is cooled down so much that further demixing is suppressed and the system ends up in a pattern of domains. Assuming that the demixing is similar to a standard spinodal decomposition, we expect the following dynamics (see, for example, Fig. 9 in Ref. [48]): For systems with a low Ti concentration, $x \gg x_c$, small and rather spherical domains of a Ti-rich phase form that are strongly separated. With time the number of domains reduces as the domains get larger. For systems with a high amount of Ti, $x \ll x_c$ the system develops similarly, but now with isolated Ti-poor domains embedded in a Ti-rich phase. If x is in the range of x_c, elongated, bent domains of Ti-rich and Ti-poor phases are interwoven. This structure is particularly complex. The lengthscale of the stripe-like domains grows with time. As the system cools down, the dynamics comes to a rest.

6. Transport

The concentration x of Mn (Sc) influences the transport properties of the alloys. We use the results obtained from our calculations for a qualitative discussion of resulting transport properties.

6.1. CoTi$_{1-x}$Mn$_x$Sb

The meanfield calculations predict a critical temperature T_c at a concentration $x_c \simeq 0.45$. Values of x_c below 0.5 have also been obtained for other half-Heusler alloys $CoTi_{1-x}Y_xSb$ ($Y = V, Cr, Fe, Cu$) [45].

Experimental measurements of $CoTi_{1-x}Mn_xSb$ have shown that adding Mn to the semiconductor CoTiSb results in a conducting material [14]. This is in agreement with our calculations, which show that the Fermi energy is located in the middle of a DOS peak for one of the spin channels. The dependence of the resistivity $\rho = \sigma^{-1}$ on the concentration x has been investigated in more detail for the magnetic material $CoV_{1-x}Mn_xSb$ [28], which is similar to $CoTi_{1-x}Mn_xSb$. This material shows metallic behavior for $0 < x < 0.3$ and $x > 0.5$. For concentrations in between, the resistivity increases strongly as the temperature goes to 0 K.

One explanation of this observation is the following: In the presence of a coexistence region, the most elongated domains with the most complex shapes of the domain boundaries occur for concentrations close to x_c. On a mesoscopic scale, the domain boundaries may be seen as a random perturbation of the ideal periodic lattice. A suitably strong random perturbation of the periodicity may lead to a localization of electrons. In spite of a finite electronic DOS at the Fermi level, localized electrons have to overcome an energy barrier E_a in order move to a neighboring site. As a consequence, the electrical conductivity σ gets proportional to $\exp(-E_a/kT)$ for suitably small temperatures and the material becomes a semiconductor [49–51]. Unfortunately, no low temperature measurements of $CoTi_{1-x}Mn_xSb$ conductivity have been performed, so far. Thus we do not know if localization of electrons is also present for this material.

The experimental study of the magnetic behavior of $CoV_{1-x}Mn_xSb$ shows that the spontaneous magnetization follows a linear increase with Mn concentration, but a sudden increase in the Curie temperature is reported near $x = 0.4$. We suggest that this sharp increase in the Curie temperature coincides with the lowest concentration at which the Mn-rich phase percolates, resulting in a long-range correlation of the magnetic moments, even at higher temperatures.

6.2. CoTi$_{1-x}$Sc$_x$Sb

The conductivity of $CoTi_{1-x}Sc_xSb$ has been measured experimentally for two Sc concentrations, $x = 0.05$ [16] and $x = 0.1$ [45]; at $x = 0.05$ the conductivity shows a semiconductor behavior while at $x = 0.1$ a metallic conductivity is measured. In our calculated DOS for different Sc concentrations we have found that with increasing Sc, the Fermi level moves away from the band gap into a region of finite DOS. Accordingly, the material will change from semiconducting to metallic. So far, no measurements have been performed for $x \simeq x_c$ and so it is unclear if there is a decrease of the conductivity due to localized electrons in this region. The effect would be of great interest for thermoelectric applications: The power factor is given by $P = \sigma S^2$. In the Mott approximation, the Seebeck coefficient is proportional to σ^{-1} such that a decrease of σ may lead to an increase of the power factor. In general, the Seebeck coefficient is a more complex function, which is composed of contributions from the different phases, as it has been showed in a related publication [52].

7. Conclusions

Motivated by experimental results showing phase separations in CoSb-based half-Heuslers alloys, we studied the structure and

the corresponding electronic properties of the half-Heusler alloys $CoTi_{1-x}Z_xSb$ with $Z =$ Mn, Sc for a variety of different concentrations x of element Z by means of a combined cluster expansion procedure and first-principle calculations. For $CoTi_{1-x}Mn_xSb$, also magnetic properties have been investigated. For both materials, $CoTi_{1-x}Z_xSb$ and $CoTi_{1-x}Mn_xSb$, a demixing of the elements in the (Ti, Z) sublattice reduces the energy.

Co(Ti,Mn)Sb is half-metallic and magnetic, even for low amounts of manganese. For a homogeneous distribution of manganese, the Fermi energy lies in a large band gap in the spin-down channel. In the spin-up channel the gap is moved to higher energies and the DOS forms a peak around E_F. In energetically favored configurations, with Mn-rich and Mn-free domains, the gap in the down channel is smaller; in the up channel the peak is reduced and the band gap has vanished. The peak and the closing of the gap in the spin-up channel are found for all transition metal atoms in the Mn-rich region, while the Mn-free region is semiconducting. As a consequence, a homogeneous phase would present a higher efficiency for spin-filtering than a phase separated phase. However, fabrication of homogeneous samples appears to be difficult as Ti and Mn atoms tend to demix. In addition we found that the distribution of the magnetic moments on the elements changes with the formation of domains.

In the case of $CoTi_{1-x}Sc_xSb$, the demixing into domains is beneficial for thermoelectric applications, since the domain boundaries reduce the heat conductivity. However, we find that also the electronic properties are not homogeneous and atoms of the same species have different characters depending on their position within the structure. It has been shown experimentally [16] that small concentrations of Sc lead to a decrease of the heat conductivity for $0 < x \leq 0.05$. For $x = 20\%$ the heat conductivity increases and the electrical conductivity increases, while the Seebeck coefficient gets very low. This matches well with our findings that for $x = 0.125$, the bottom of the band gap is still close to the Fermi energy, while for $x = 25\%$ it is distinctly larger. From a theoretical point of view, the consequences in the electrical conductivity and the Seebeck coefficient remain to be studied in phase separated systems on a large scale.

The tendency of $CoTi_{1-x}Sc_xSb$ and $CoTi_{1-x}Mn_xSb$ to demix and form nanodomains makes them interesting for fundamental aspects and applications. Properties of domains on a larger scale and their temperature dependence should be studied in the future. The formation of nanodomains with distinctly different electronic properties should also be studied in more detail with respect to its charge transport properties. Results should be compared with the models [20,44] for systems with a spatially dependent conductivity. The effects observed for the two studied systems should also be found in other more complex compositions, so that our findings are a first step towards a comprehensive understanding of the large class of half-Heusler alloys that demix into nanodomains.

Acknowledgments

References

[1] F. Heusler, W. Starck, E. Haupt, et al., Verh. D. DPG 5 (1903) 220.
[2] J. Heusler, D. DPG 5 (1903) 219.
[3] L. Offernes, P. Ravindran, A. Kjekshus, J. Alloys Compd. 439 (2007) 37.
[4] H.C. Kandpal, C. Felser, R. Seshadri, J. Phys. D. Appl. Phys. 39 (2006) 776.
[5] J. Tobola, J. Pierre, J. Alloys Compd. 296 (2000) 243.
[6] D. Kieven, R. Klenk, S. Naghavi, C. Felser, T. Gruhn, Phys. Rev. B 81 (2010) 075208.
[7] Thomas Gruhn, Phys. Rev. B 82 (2010) 125210.
[8] Z. Bai, L. Shen, G. Han, Y. Ping, SPIN 2 (2012) 1230006.
[9] S. Chadov, X. Qi, J. Kübler, G.H. Fecher, C. Felser, S.C. Zhang, Nat. Mater 9 (2010) 541.
[10] G. Jeffrey Snyder, E.S. Toberer, Nat. Mat. 7 (2008) 105.
[11] L.L. Wang, L. Miao, Z.Y. Wang, W. Wie, R. Xiong, H.J. Liu, J. Shi, X.F. Tang, J. Appl. Phys. 105 (2009) 013709.
[12] Wei Lu, Charles M. Lieber, Nat. Mat. 6 (2007) 841.
[13] J. Barth, B. Balke, G.H. Fecher, H. Stryhanyuk, A. Gloskovskii, S. Naghavi, C. Felser, J. Phys. D. Appl. Phys. 42 (2009) 185401.
[14] T. Graf, P. Klaer, J. Barth, B. Balke, H.-J. Elmer, C. Felser, Scr. Mater 63 (2010) 1216.
[15] M. Schwall, Heusler Compunds for Thermoelectric Applications, Johannes Gutenberg-Universität, Mainz, Germany, 2014. Doctoral thesis.
[16] S. Ouardi, Gerhard H. Fecher, C. Felser, M. Schwall, S.S. Naghavi, A. Gloskovskii, B. Balke, J. Hamrle, K. Postava, J. Pistora, S. Ueda, K. Kobayashi, Phys. Rev. B 86 (2012) 045116.
[17] R.A. de Groot, F.M. Mueller, P.G. van Engen, K.H.J. Buschow, Phys. Rev. Lett. 50 (1983) 2024.
[18] A. Slebarski, A. Jezierski, S. Lütkehoff, M. Neumann, Phys. Rev. B 57 (1998) 6408.
[19] B.R.K. Nanda, I. Dasgupta, J. Phys. Condens. Matter 17 (2005) 5037.
[20] L. Chaput, J. Tobola, P. Pecheur, H. Scherrer, Phys. Rev. B 73 (2006) 045121.
[21] B. Alling, M. Ekholm, I.A. Abrikosov, Phys. Rev. B 77 (2008) 144414.
[22] B. Balke, G.H. Fecher, A. Gloskovskii, J. Barth, K. Kroth, C. Felser, R. Robert, A. Weidenkaff, Phys. Rev. B 77 (2008) 045209.
[23] Zhiyong Zhu, Yingchun Cheng, Udo Schwingenschlögl, Phys. Rev. B 84 (2011) 113201.
[24] D. Orgassa, H. Fujiwara, T.C. Schulthess, W.H. Butler, Phys. Rev. B 60 (1999) 13237.
[25] S. Sharma, S.K. Pandey, J. Phys. Condens. Matter 26 (2014) 215501.
[26] J. Barth, Gerhard H. Fecher, B. Balke, Siham Ouardi, Tanja Graf, C. Felser, A. Shkabko, A. Weidenkaff, P. Klaer, H.J. Elmers, H. Yoshikawa, S. Ueda, K. Kobayashi, Phys. Rev. B 81 (2010) 064404.
[27] J. Krez, J. Schmitt, G.J. Snyder, C. Felser, W. Hermes, M. Schwind, J. Mat. Chem. A 2 (2014) 13513.
[28] K. Kaczmarska, J. Pierre, J. Tobola, R.V. Skolozdra, Phys. Rev. B 60 (1999) 373.
[29] H.M. Huang, S.J. Luo, K.L. Yao, Phys. B 406 (2011) 1368.
[30] I. Galanakis, P.H. Dederichs, N. Papanikolaou, Phys. Rev. B 66 (2002) 134428.
[31] Tran Quang Hung, Mai Suan Li, Marek Cieplak, J. Magn. Magn. Mater. 138 (1994) 153.
[32] V. Ksenofontov, G. Melnyk, M. Wojcik, Sabine Wurmehl, K. Kroth, S. Reiman, P. Blaha, C. Felser, Phys. Rev. B 74 (2006) 134426.
[33] A. van de Walle, G. Ceder, J. Phase Equilib. 23 (2002) 348.
[34] M. Stone, J. Roy, Stat. Soc. B Met. 36 (1974) 111.
[35] A. van de Walle, ATAT User Guide, 2013.
[36] G.D. Garbulsky, G. Ceder, Phys. Rev. B 51 (1995) 67.
[37] P.E. Blöchl, Phys. Rev. B 50 (1994) 17953.
[38] G. Kresse, D. Joubert, Phys. Rev. B 59 (1999) 1758.
[39] H.J. Monkhorst, J.D. Pack, Phys. Rev. B 13 (1976) 5188.
[40] J. Kübler, A.R. Williams, C.B. Sommers, Phys. Rev. B 28 (1983) 1745.
[41] M. Schwall, Leslie M. Schoop, Siham Ouardi, B. Balke, C. Felser, Peter Klaer, Hans-Joachim Elmers, Adv. Funct. Mat. 22 (2012) 1822.
[42] J. Kübler, Phys. B 127 (1984) 257.
[43] S. Ouardi, Gerhard H. Fecher, B. Balke, X. Kozina, G. Stryganyuk, C. Felser, S. Lowitzer, D. Ködderitzsch, H. Ebert, E. Ikenaga, Phys. Rev. B 82 (2010) 085108.
[44] Mal-Soon Lee, Ferdinand P. Poudeu, S.D. Mahanti, Phys. Rev. B 83 (2011) 085204.
[45] J. Miranda Mena, E. Rausch, S. Ouardi, T. Gruhn, G.H. Fecher, H.G. Schoberth, H. Emmerich, C. Felser, J. Electron. Mater. (2015) (accepted).
[46] T. Jaeger, P. Holuj, C. Mix, C. euler, M. Haydee Aguirre, S. Populoh, A. Weidenkaff, G. Jakop, Semicond. Sci. Technol. 29 (2014) 124003.
[47] Do-young Jung, Ken Kurosaki, Chang-eun Kim, Hiroaki Muta, Shinsuke Yamanaka, J. Alloys Compd. 489 (2010) 328.
[48] Y.C. Li, R.P. Shi, C.P. Wang, X.J. Liu, Y. Wang, Model. Simul. Sci. Enf. 20 (2012) 075002.
[49] N.F. Mott, Philos. Mag. 19 (1969) 835.
[50] N.F. Mott, Electronic Properties in Non-crystalline Materials, Clarendon Press, Oxford, 1979. ISBN 019851288.
[51] A.L. Efros, B.I. Shklovskii, J. Phys. C. Solid State Phys. 8 (1975) L49.
[52] Joachim Sonntag, Phys. Rev. B 73 (2006) 045126.